Angular Frequency Dynamic-Based Control Technique of a Grid-Interfaced Converter Emulated by a Synchronous Generator

Majid Mehrasa
C-MAST/UBI
Portugal

Amir Sepehr, Edris Pouresmaeil, Jorma Kyyrä
Dep. of Elec. Eng. and Auto.,
Aalto University,
Finland

Mousa Marzband
Dep. of Mech. and Elec. Eng.
Northumbria University,
UK

João P. S. Catalão
INESC TEC and FEUP, Porto,
C-MAST/UBI, Covilha, and
INESC-ID/IST-UL, Lisbon,
Portugal

***Abstract*—In this paper, an angular frequency dynamic-based control technique is proposed to control interfaced converters between the power grid and renewable energy sources. The proposed control technique can guarantee a stable operation of power grid under high penetration of renewable energy resources through providing the required inertia properties. The synchronous generator characteristics combined with the basic dynamic model of the interfaced converter can shape a second order derivative of the grid angular frequency consisting of converter power and virtual mechanical power derivative with embedded virtual inertia to prevent instability from the power grid as well as to generate active and reactive power with appropriate inertia. Simulation analyses are performed in Matlab/Simulink to attest the high performance of the proposed control technique.**

Keywords—High penetration, synchronous generator, angular frequency dynamic, power grid stability, virtual inertia, virtual mechanical power.

I. Introduction

Using renewable energy resources has been attracted more attention because of their superiority especially environmental reasons and renewability features in recent years [1]-[3].

Mimicking the synchronous generator (*SG*) features which are combined with various novel control techniques designed for power converters in renewable energy resources applications [4] has been considered recently to increase the stability margin of the power grid under high penetration of renewable energy resources [5].

Several papers have focused on defining the behaviors of SG in the way to be seen in their proposed control technique performance [6]-[13].

Reference [6] has discussed about the virtual synchronous generator (*VSG*) technology employed in integration of *PV* and wind power (*WP*) generators, power electronics transformer and flexible ac and dc transmission.

To make clear the differences between inverters and real synchronous generators, a virtual synchronous generator-based control strategy is designed in [7] to emulate and analyze the swing and power equations.

By the help of $V^2-P-\omega$ characteristic and the V^2-P droop control, a virtual synchronous generator (*VSG*) control method has been proposed in [8] to provide the low-frequency oscillations damping performance with modelling both rotational inertia and governor parts.

In [9], by using a non-ideal proportional-resonant (*PR*) controller and *SG* features embedded in swing equation, a synchronous active proportional resonant-based control strategy has been proposed to control a grid-interfaced converter for high penetration of RERs into the power grid.

Reference [10] has investigated the virtual inertia of distributed power system that is implemented by grid-connected power converters for reaching the ever-decreasing inertia condition. Reference [11] has proposed a power-based control technique to force the interfaced power converter to have the inherent features of synchronous power generators by injecting both active and reactive power into the power grid. Using virtual synchronous generator-based control strategy in references [12] and [13] have been considered to achieve stability in presence of a total capacity of the grid-connected converters greater than conventional synchronous generators.

A control technique based on grid angular frequency second order dynamic is proposed in this paper for an interfaced converter to make the power grid stable with high penetration of renewable energy resources. The differences between the methods presented in [6]-[13] are mainly due to the ways of inserting the SG features into the basic dynamic models of used converters as well as their related evaluations.

The proposed control strategy consists of synchronous generator characteristics and the basic dynamic model of the interfaced converter. In the designed control technique, the errors of virtual mechanical power and second order angular frequency are considered. Simulation results show that the proposed control technique can keep the power grid stable in the presence of active and reactive power variations due to the high penetration of *RERs*.

II. The Proposed Control Technique

In order to control the interfaced converters with a suitable control strategy, an appropriate dynamic model should be first extracted.

Edris Pouresmaeil acknowledges the support by the Department of Electrical Engineering and Automation at Aalto University, Finland. Moreover, João P. S. Catalão acknowledges the support by FEDER funds through COMPETE 2020 and by Portuguese funds through FCT, under Projects SAICT-PAC/0004/2015 - POCI-01-0145-FEDER-016434, POCI-01-0145-FEDER-006961, UID/EEA/50014/2013, UID/CEC/50021/2013, UID/EMS/00151/2013, and 02/SAICT/2017 - POCI-01-0145-FEDER-029803, and also funding from the EU 7th Framework Programme FP7/2007-2013 under GA no. 309048.

978-1-5386-5326-5/18/$31.00 ©2018 IEEE

According to Fig.1, the basic mathematical model of the interfaced converter can be written as,

$$\begin{cases} L\dfrac{di_d}{dt}+Ri_d-\omega Li_q-u_d v_{dc}+v_d=0 \\ L\dfrac{di_q}{dt}+Ri_q+\omega Li_d-u_q v_{dc}+v_q=0 \\ C\dfrac{dv_{dc}}{dt}+u_d i_d+u_q i_q+i_{dc}=0 \end{cases} \quad (1)$$

where L, R, C are the inductance, resistance and input capacitance of interfaced converter, respectively. Variables i_{dq}, v_{dq}, u_{dq} are output currents, output voltages, and switching functions of interfaced converter in d-q reference frame, and i_{dc} and v_{dc} are the dc-link current and voltage, respectively. The state variable of ω is the angular frequency of interfaced converter. To achieve an active and reactive power-based dynamic model, the currents of $i_d=P/v_d$ and $i_q=-Q/v_d$ are substituted into (1) that result in:

$$\begin{aligned} &\frac{L}{R}\frac{dP}{dt}+P+\frac{\omega L}{R}Q-u_d P_{c1}+P_d=0 \\ &\frac{L}{R}\frac{dQ}{dt}+Q-\frac{\omega L}{R}P+u_q P_{c1}-P_{dq}=0 \\ &RC\frac{dP_{c1}}{dt}+u_d P-u_q Q+P_{c2}=0 \end{aligned} \quad (2)$$

where P and Q are the active and reactive power of interfaced converter and other powers in (2) are defined as $P_{c1}=v_{dc}v_d/R$, $P_{c2}=i_{dc}v_d$, $P_{pd}=v_{d2}/R$, and $P_{pdq}=v_d v_q/R$. To reach a relationship between features of SG and active power of converter, the following swing equation are considered:

$$J\frac{d\omega}{dt}=\frac{P_m-P}{\omega} \quad (3)$$

where P_m and J are the mechanical power and moment inertia of synchronous generator. The equation (3) can be converted to (4) by applying small signal linearization to (3) that can lead to:

$$\Delta\omega=\frac{1}{\omega^* J}\cdot\frac{\Delta P_m-\Delta P}{s+\left(P_m^*-P^*\right)/\omega^{*2}J} \quad (4)$$

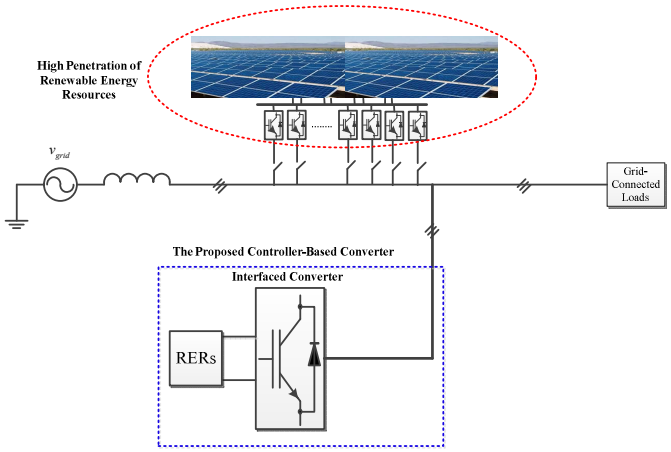

Fig.1. the general structure of considered converter in high penetration of renewable energy resources.

By rearranging (4), the error of active power can be stated as:

$$\frac{\Delta P}{s}=\frac{\Delta P_m}{s}-\left(\omega^* J+\frac{\left(P_m^*-P^*\right)}{\omega^* s}\right)\Delta\omega \quad (5)$$

where P_m^*, P^* and ω^* are the reference values of active power, mechanical power, and angular frequency, respectively. The relationship between the active and reactive power is equal to $P^2+Q^2=S^2$. Since it is assumed that the apparent power of S is constant, by applying small signal linearization into the aforementioned relationship, the error of reactive power can be rewritten as:

$$\frac{\Delta Q}{s}=-\frac{P^*}{Q^*}\frac{\Delta P_m}{s}+\frac{P^*}{Q^*}\left(\omega^* J+\frac{\left(P_m^*-P^*\right)}{\omega^* s}\right)\Delta\omega \quad (6)$$

where Q^* is the reference value of reactive power. Considering equations (4)-(6), the small signal description of the proposed system can be written as:

$$\begin{aligned} \frac{\Delta\omega}{s}&=\frac{-1/\omega^* Js}{s+\left(P_m^*-P^*\right)/\omega^{*2}J}\Delta P+ \\ &\frac{1}{\omega^* Js}\cdot\frac{1}{s+\left(P_m^*-P^*\right)/\omega^{*2}J}\Delta P_m \\ \frac{\Delta P}{s}&=-\left(\omega^* J+\frac{\left(P_m^*-P^*\right)}{\omega^* s}\right)\Delta\omega+\frac{1}{s}\Delta P_m \\ \frac{\Delta Q}{s}&=\frac{P^*}{Q^*}\left(\omega^* J+\frac{\left(P_m^*-P^*\right)}{\omega^* s}\right)\Delta\omega-\frac{P^*}{Q^*}\frac{1}{s}\Delta P_m \end{aligned} \quad (7)$$

Using following definitions for all power and angular frequency variations:

$$\Delta x=x^*-x \qquad x\in\{P,Q,P_m,\omega\} \quad (8)$$

By the use of (7) and (8), the ultimate proposed dynamic model is obtained as:

$$\begin{aligned} &\left(\omega^{*2}J\right)\frac{d\omega}{dt}+\left(P_m^*-P^*\right)\omega+\left(\omega^*\right)P-\left(\omega^*\right)P_m= \\ &\left[\omega^{*2}J\dot{\omega}^*+\left(P_m^*-P^*\right)\omega^*-\omega^* P_m^*+\omega^* P^*\right] \end{aligned} \quad (9)$$

$$\begin{aligned} &\left(\omega^{*2}P^*J\right)\frac{d\omega}{dt}+\left(P^*\left(P_m^*-P^*\right)\right)\omega \\ &-\left(\omega^* Q^*\right)Q-\left(\omega^* P^*\right)P_m \\ &=\left[\omega^{*2}P^*J\dot{\omega}^*+P^*\left(P_m^*-P^*\right)\omega^*-\omega^* P^* P_m^*-\omega^* Q^{*2}\right] \end{aligned} \quad (10)$$

To achieve an accurate zero dynamic-based analysis regarding to the proposed controller-based model, the second order derivative of the angular frequency should be driven by use of (10) and (11) as:

$$\begin{aligned} &\left(\omega^{*2}J\right)\frac{d^2\omega}{dt^2}+\left(P_m^*-P^*\right)\frac{d\omega}{dt}+\left(\omega^*\right)\frac{dP}{dt}= \\ &\frac{d\left[\begin{array}{l}\omega^{*2}J\dot{\omega}^*+\left(P_m^*-P^*\right)\omega^* \\ -\omega^* P_m^*+\omega^* P^*+\left(\omega^*\right)P_m\end{array}\right]}{dt} \end{aligned} \quad (11)$$

$$\left(\omega^{*2}P^{*}J\right)\frac{d^{2}\omega}{dt^{2}}+\left(P^{*}\left(P_{m}^{*}-P^{*}\right)\right)\frac{d\omega}{dt}-\left(\omega^{*}Q^{*}\right)\frac{dQ}{dt}$$
$$=\frac{d\begin{bmatrix}\omega^{*2}P^{*}J\dot{\omega}^{*}+P^{*}\left(P_{m}^{*}-P^{*}\right)\omega^{*}-\omega^{*}P^{*}P_{m}^{*}\\-\omega^{*}Q^{*2}+\left(\omega^{*}P^{*}\right)P_{m}\end{bmatrix}}{dt} \quad (12)$$

The proposed control technique is described in Fig. 2. Based on this figure, proportional-resonant (PR) controller is used for removing the second order angular frequency-based error. Also, the virtual mechanical power error can be found in both components of the proposed control strategy.

III. Evaluation of Second Order Angular Frequency-Based Equations

The zero dynamic of the virtual mechanical power is found in (11) and (12). Moreover, it can be realized from (11) and (12) that the zero dynamics of the active and reactive power can highly impact on the angular frequency variations.

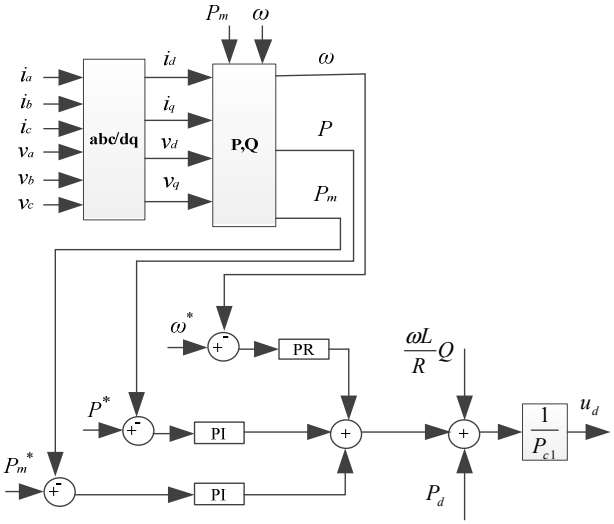

(a)

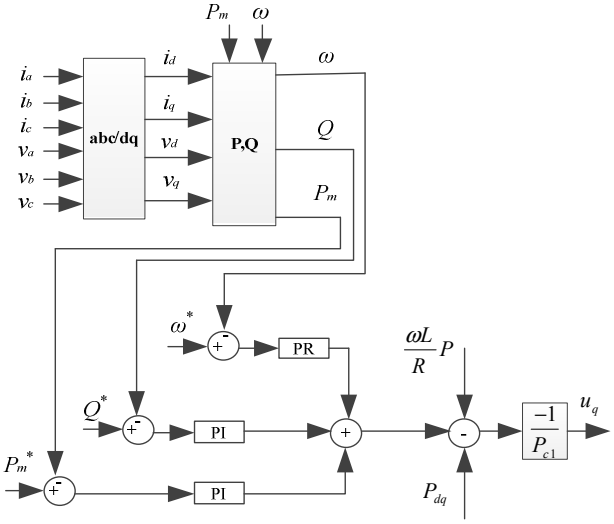

(b)

Fig.2. General structure of the proposed control technique.

By obtaining *dP/dt* and *dQ/dt* from the first and second terms of (2) respectively, and substituting the results into (11) and (12), two accurate zero dynamic models for the grid angular frequency can be achieved as:

$$\left(\omega^{*2}J\right)\frac{d^{2}\omega}{dt^{2}}+\left(P_{m}^{*}-P^{*}\right)\frac{d\omega}{dt}-\left(\omega^{*}Q\right)\omega= \quad (13)$$
$$k_{1}\left(\begin{matrix}R,L,J,\dot{J},\omega^{*},\dot{\omega}^{*},\ddot{\omega}^{*},P_{m}^{*},P^{*}\\,\dot{P}_{m}^{*},\dot{P}^{*},P,P_{d},P_{c1},u_{d},\end{matrix}\right)$$

$$\omega^{*2}P^{*}J\frac{d^{2}\omega}{dt^{2}}+P^{*}\left(P_{m}^{*}-P^{*}\right)\frac{d\omega}{dt}-\left(\omega^{*}Q^{*}P\right)\omega= \quad (14)$$
$$k_{2}\left(\begin{matrix}R,L,J,\dot{J},\omega^{*},\dot{\omega}^{*},\ddot{\omega}^{*},P_{m}^{*},\\P^{*},\dot{P}_{m}^{*},\dot{P}^{*},Q,Q^{*},P_{d},P_{c1},P_{dq},u_{q}\end{matrix}\right)$$

where,

$$k_{1}\left(R,L,J,\dot{J},\omega^{*},\dot{\omega}^{*},\ddot{\omega}^{*},P_{m}^{*},P^{*},\dot{P}_{m}^{*},\dot{P}^{*},P,P_{d},P_{c1},u_{d},\right) \quad (15)$$
$$\frac{d\left(\omega^{*2}J\dot{\omega}^{*}+\left(P_{m}^{*}-P^{*}\right)\omega^{*}-\omega^{*}P_{m}^{*}+\omega^{*}P^{*}\right)}{dt}$$
$$+\frac{\omega^{*}RP}{L}-\frac{\omega^{*}Ru_{d}P_{c1}}{L}+\frac{\omega^{*}RP_{d}}{L}+\frac{\omega^{*}dP_{m}}{dt}$$
$$k_{2}\left(\begin{matrix}R,L,J,\dot{J},\omega^{*},\dot{\omega}^{*},\ddot{\omega}^{*},P_{m}^{*},P^{*},\dot{P}_{m}^{*}\\,\dot{P}^{*},Q,Q^{*},P_{d},P_{c1},P_{dq},u_{q}\end{matrix}\right)= \quad (16)$$
$$\frac{d\left(\omega^{*2}P^{*}J\dot{\omega}^{*}+P^{*}\left(P_{m}^{*}-P^{*}\right)\omega^{*}-\omega^{*}P^{*}P_{m}^{*}-\omega^{*}Q^{*2}\right)}{dt}-$$
$$\frac{\omega^{*}Q^{*}RQ}{L}-\frac{\omega^{*}Q^{*}Ru_{q}P_{c1}}{L}+\frac{\omega^{*}Q^{*}RP_{dq}}{L}+\frac{\omega^{*}P^{*}dP_{m}}{dt}$$

Except for the state variables involved with the converter operating conditions, both virtual inertia and mechanical power can highly impact on performance of the grid angular frequency as demonstrated in (15) and (16). By solving the differential equations of (13) and (14), the closed-loop frequencies can be achieved as:

$$s_{1}=\frac{-\frac{\left(P_{m}^{*}-P^{*}\right)}{\omega^{*2}J}+\sqrt{\left(\frac{\left(P_{m}^{*}-P^{*}\right)}{\omega^{*2}J}\right)^{2}+\frac{4Q}{\omega^{*}J}}}{2} \quad (17)$$
$$s_{2}=\frac{-\frac{\left(P_{m}^{*}-P^{*}\right)}{\omega^{*2}J}-\sqrt{\left(\frac{\left(P_{m}^{*}-P^{*}\right)}{\omega^{*2}J}\right)^{2}+\frac{4Q}{\omega^{*}J}}}{2}$$

$$s_{3}=\frac{-\frac{\left(P_{m}^{*}-P^{*}\right)}{\omega^{*2}J}+\sqrt{\left(\frac{\left(P_{m}^{*}-P^{*}\right)}{\omega^{*2}J}\right)^{2}+4\frac{\left(Q^{*}P\right)}{\omega^{*}P^{*}J}}}{2} \quad (18)$$
$$s_{4}=\frac{-\frac{\left(P_{m}^{*}-P^{*}\right)}{\omega^{*2}J}-\sqrt{\left(\frac{\left(P_{m}^{*}-P^{*}\right)}{\omega^{*2}J}\right)^{2}+4\frac{\left(Q^{*}P\right)}{\omega^{*}P^{*}J}}}{2}$$

Considering (13)-(14) and (17)-(18), the grid angular frequency can be achieved as:

$$\omega = A + \frac{0.5k_1}{\left(\omega^{*2}J\right)\left(\sqrt{\left(\frac{\left(P_m^* - P^*\right)}{\omega^{*2}J}\right)^2 + \frac{4Q}{\omega^* J}}\right)}\left[\frac{1}{s_2}e^{s_2 t} - \frac{1}{s_1}e^{s_1 t}\right] + \frac{0.5k_2}{\omega^{*2}P^*J\left(\sqrt{\left(\frac{\left(P_m^* - P^*\right)}{\omega^{*2}J}\right)^2 + 4\frac{\left(Q^*P\right)}{\omega^* P^* J}}\right)}\left[\frac{1}{s_4}e^{s_4 t} - \frac{1}{s_3}e^{s_3 t}\right] \quad (19)$$

Various states of (19) are drawn in Fig. 3. As can be seen from this figure, changing the virtual inertia can be utilized to reach a desired value for the angular frequency of grid. For positive values of s_1, s_2, s_3, and s_4, two unstable responses in Fig. 3 are achieved. But in the cases of stable responses, the magnitude of fluctuations of the response is noticeably decreased as shown in Fig.3 as blue color. On the other hand, very low and high values of the virtual inertia can lead to the non-compensable transient reaction of the grid angular frequency. The low-high values of the virtual inertia can provide appropriate respond instead.

IV. Simulation Results

The proposed angular frequency dynamic-based control strategy is evaluated by some simulation results through MATLAB/SIMULINK environment. The system parameters used in the simulation are specified in Table I.

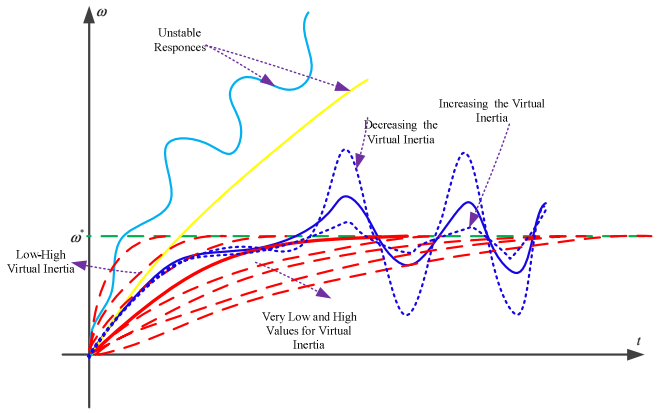

Fig. 3. The virtual inertia effects on the grid angular frequency.

TABLE I: Simulation Parameters

Parameter	Value	Parameter	Value
dc-link Voltage (v_{dc})	850 V	J	1e3 kg.m^2
Phase ac voltage	220 V	Pm	3.3 kW
Fundamental frequency	50 Hz	P	3 kW
Switching frequency	10 kHz	Q	2 kVAr
Interface converter resistance	0.1 Ohm	Interface converter inductance	45 mH

A. Decrement of active and reactive power injected into power grid

It is assumed that the active and reactive power injected into power grid is decreased at t=0.1s. This decrement leads to rising grid frequency and decreasing grid voltage magnitude as shown in Fig. 4 and 5, respectively. It can be understood from Fig. 4 and 5 that the proposed control strategy is able to provide stable values for both grid frequency and voltage magnitude in steady state condition. Also, after dynamic change, both grid frequency and voltage magnitude can appropriately follow their reference values. As it can be seen from Fig. 4 and 5, the appropriate operation of proposed control technique can cause the grid frequency and voltage magnitude to reach its desired value with a very good transient response. To compensate these variations, the proposed control technique-based interfaced converter is set to supply the needed power of the grid based on Fig. 6 and 7. After power decrement at t=0.1s, both grid frequency and voltage magnitude are affected by this power change. Fig. 6 and 7 show that no change happens for the active and reactive power of interfaced converter until t=0.25s. According to Fig. 6 and 7, interfaced converter increases its power generation to compensate the needed active and reactive power of grid.

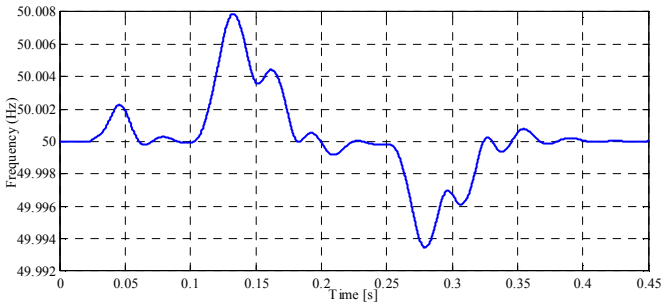

Fig. 4. The grid frequency.

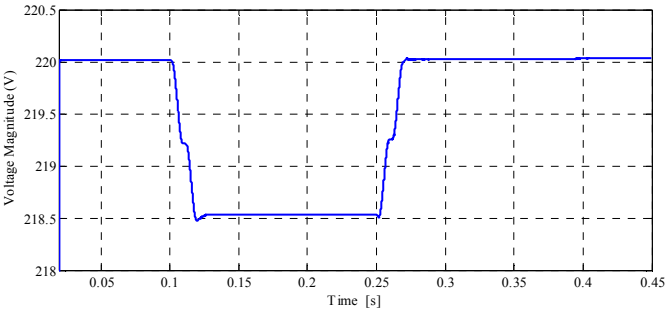

Fig. 5. The grid voltage magnitude.

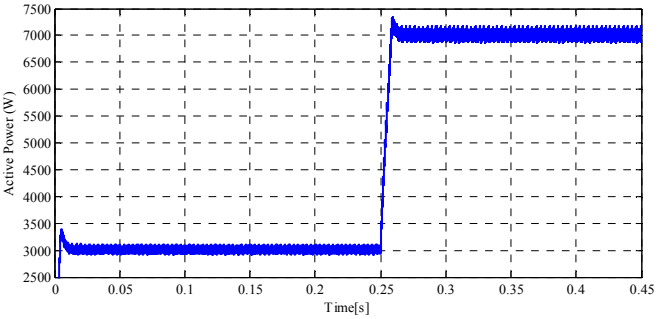

Fig. 6. The active power of proposed control technique-based interfaced converter.

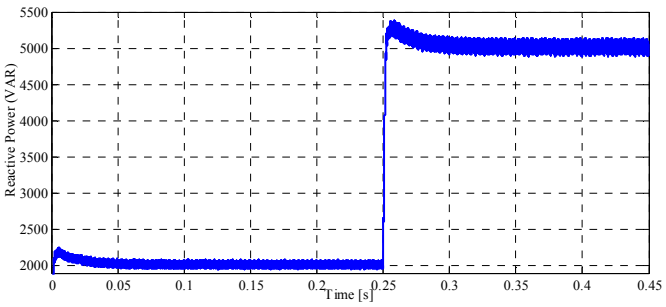

Fig. 7. The reactive power of proposed control technique-based interfaced converter.

V. CONCLUSION

A second-order angular frequency dynamic-based control technique has been designed in this paper to provide stable values for grid frequency and voltage magnitude under high penetration of renewable energy resources into the power grid. Based on the mathematical model of the interfaced converter and the dynamic characteristics of the synchronous generator, the so-called swing equation, the proposed control technique has been introduced. It can be considered as future work that more interfaced converters in the parallel connection can utilize this control technique in a microgrid structure. Simulation results confirmed that the proposed control technique can guarantee a stable operating condition for the power grid under high penetration of RESs.

REFERENCES

[1] Nasirian V, Shafiee Q, Guerrero JM, Lewis FL, Davoudi A. Droop-Free Distributed Control for AC Microgrids. IEEE Transactions on Power Electronics 2016; 31 (2): 1600 – 1617.

[2] M. Mehrasa, E. Pouresmaeil, H. Mehrjerdi, B. N. Jørgensen, J. P. S. Catalão, ‘‘Control technique for enhancing the stable operation of distributed generation units within a microgrid,’’ Energy Conversion and Management, vol. 97, pp. 362–373, 2015.

[3] E. Pouresmaeil, H.R. Shaker, M. Mehrasa, M.A. Shokridehaki, E.M.G. Rodrigues, and J.P.S Catalão, “Integration of renewable energy for the harmonic current and reactive power compensation,’’ Powereng, Sep. 2015.

[4] Pouresmaeil E, Mehrasa M, Erdinc O, Catalao JPS. A Control Algorithm for the Stable Operation of Interfaced Converters in Microgrid Systems. Innovative Smart Grid Technologist Conference Europe (ISGT-Europe) 2014; 1-6.

[5] S. Tan, Q. Lv, H. Geng, G. Yang, ‘‘An Equivalent Synchronous Generator Model for Current-Controlled Voltage Source Converters Considering the Dynamic of Phase-locked-loop,’’ IECON, pp. 2235-40, 2016.

[6] X. Kong, J. Pan, X. Gong, P. Li, ‘‘Emulating the features of conventional generator with virtual synchronous generator technology: an overview,’’ The Journal of Engineering, vol. 2017, no. 13, pp. 2135 - 2139, 2017.

[7] M. Li, Y. Wang, N. Xu, Y. Liu, W. Wang, H. Wang, W. Lei, ‘‘A Novel Virtual Synchronous Generator Control Strategy Based on Improved Swing Equation Emulating and Power Decoupling Method,’’ ECCE, pp. 1-7, February 2016.

[8] Y. Cao, W. Wang, Y. Li, Y. Tan, C. Chen, L. He, U. Häger, C. Rehtanz, ‘‘A Virtual Synchronous Generator Control Strategy for VSC-MTDC Systems,’’ IEEE Transactions on Energy Conversion, vol. 33, no. 2, pp. 750 - 761, June 2018.

[9] M. Mehrasa, R. Godina, E. Pouresmaeil, I. Vechiu, R. L. Rodríguez, J. P. S. Catalão, ‘‘Synchronous active proportional resonant-based control technique for high penetration of distributed generation units into power grids,’’ Innovative Smart Grid Technologies Conference Europe (ISGT-Europe), 2017 IEEE PES, pp. 1-6, January 2018.

[10] J. Fang, H. Li, Y. Tang, F. Blaabjerg ‘‘Distributed Power System Virtual Inertia Implemented by Grid-Connected Power Converters,’’ IEEE Transactions on Power Electronics (Early Access), DOI: 10.1109/TPEL.2017.2785218, pp. 1 - 1, Dec 2017.

[11] E. Pouresmaeil, M. Mehrasa, R. Godina, I. Vechiu, R. L. Rodríguez, J. P. S. Catalão, ‘‘Double synchronous controller for integration of large-scale renewable energy sources into a low-inertia power grid,’’ Innovative Smart Grid Technologies Conference Europe (ISGT-Europe), 2017 IEEE PES, pp. 1-6, January 2018.

[12] T. Zheng, L. Chen, Y. Guo, S. Mei, ‘‘Comprehensive control strategy of virtual synchronous generator under unbalanced voltage conditions,’’ IET Generation, Transmission & Distribution, vol. 12, no. 7, pp. 1621 - 1630, March 2018.

[13] Y. Hirase, K. Sugimoto, K. Sakimoto, T. Ise, ‘‘Analysis of Resonance in Microgrids and Effects of System Frequency Stabilization Using a Virtual Synchronous Generator,’’ IEEE Journal of Emerging and Selected Topics in Power Electronics, vol. 4, no. 4, pp. 1287 - 1298, June 2016.